IEEE Access
Multidisciplinary ⋮ Rapid Review ⋮ Open Access Journal

Received 21 March 2024, accepted 8 May 2024, date of publication 13 May 2024, date of current version 20 May 2024.

Digital Object Identifier 10.1109/ACCESS.2024.3400153

RESEARCH ARTICLE

Optimization of Radial Electrodynamic Bearing Using Artificial Neural Network

D. K. SUPREETH, SIDDAPPA I. BEKINAL, AND R. C. SHIVAMURTHY
Department of Mechanical and Industrial Engineering, Manipal Institute of Technology, Manipal Academy of Higher Education, Manipal, Udupi, Karnataka 576104, India

Corresponding author: Siddappa I. Bekinal (siddappa.bekinal@manipal.edu)

This work was supported in part by Indian Science, Technology, and Engineering facilities Map (I-STEM) Program funded by the Office of the Principal Scientific Adviser to the Government of India; and in part by Manipal Institute of Technology, Manipal Academy of Higher Education, Manipal.

ABSTRACT This article focuses on the prediction of essential bearing characteristics and optimization of electrodynamic bearing (EDB). Initially, a sensitivity analysis was conducted, manipulating key design parameters to assess their impact on electric pole frequency (ω), stiffness (k), and damping (c). Subsequently, the data derived from the sensitivity analysis was employed as input for training an artificial neural network (ANN) model. The ANN model was developed and trained with six inputs using various algorithms and different hidden neuron configurations to forecast essential bearing characteristics. Three distinct artificial neural network models (for c, k, and ω) were created. Notably, Bayesian Regularization with 10 hidden neurons exhibited superior performance, demonstrating the least average error. In the final stage, the ANN model was utilized to optimize the EDB through the Bonobo optimization algorithm in MATLAB. The optimization results were validated using COMSOL Multiphysics, where essential bearing characteristics were determined by fitting an analytical model to simulation outcomes. These outcomes were then compared with the ANN model predictions, affirming the applicability of ANN models in both predicting and optimizing EDB performance.

INDEX TERMS Artificial neural network, electrodynamic bearing, optimization.

I. INTRODUCTION

Magnetic bearings fall into the category of bearings that provide rotor support through the utilization of electromagnetic forces generated by the interaction between rotor and stator magnets. As there is no physical contact between components of rotor and stator, friction is eliminated, resulting in decreased wear and a longer overall lifespan. Subsequently, maintenance cost is reduced, due to reduction wear. Furthermore, lubrication is unnecessary, owing to the absence of contact which makes magnetic bearing useful for operation in high-temperature conditions [1].

For industrial applications active magnetic bearings (AMB) are widely utilized, owing to the fact that they can adjust their stiffness and damping for any specific requirements. Also, during operation, AMB can adapt to any changes in rotor speed and its position.

This adaptability allows them to essentially alleviate problems related to shaft critical frequencies, making them highly adaptable and valuable in industrial applications. However, because of the presence of sensors, controllers, and power electronics, they are not suitable for applications demanding compactness and cost-effectiveness.

Conversely, passive magnetic bearings don't utilize sensors, controllers, or power electronics to achieve rotor suspension. The rotor is levitated using permanent magnets. However, it's worth noting Earnshaw's theorem, which states that stable rotor suspension cannot be achieved with static magnetic fields alone. This theorem suggests that alternative approaches must be employed, at least for one degree of freedom, in order to achieve fully passive magnetic levitation [2]. Passive levitation is possible either employing

The associate editor coordinating the review of this manuscript and approving it for publication was Jinquan Xu.

© 2024 The Authors. This work is licensed under a Creative Commons Attribution-NonCommercial-NoDerivatives 4.0 License.
For more information, see https://creativecommons.org/licenses/by-nc-nd/4.0/

superconductors [3], mechanical bearings [4], and electromagnets [5]. The primary drawback of passive magnetic bearings lies in their low damping characteristics, a limitation that can be mitigated through the implementation of eddy current dampers for improvement [6]. Hence EDB are a class of passive magnetic bearings in which rotor is levitated due to the Lorentz force generated by the movement of conductor in a magnetic field [7]. EDB are considered an attractive alternative due to their capability to impart passive positive stiffness without introducing any negative stiffness in any direction [8]. EDB comes in two distinct types: radial bearings, which enable control over the rotor's radial degrees of freedom, and axial bearings, which facilitate axial levitation. To characterize radial and axial EDB, various models have been developed, covering scenarios in quasi-static conditions [9], [10], [11], [12], [13], where spin speed and eccentricity are held constant, as well as dynamic conditions [14], [15], [16], [17]. Given the significance of stiffness and electric pole frequency in EDB design, various sensitivity analyses have been conducted to gain insights into critical geometric parameters [18]. One drawback of EDB is their susceptibility to various types of instabilities. A primary concern associated with EDB revolves around the generation of rotational damping forces due to the conductor's rotational motion, leading to the rotor's instability. Literature has put forward several solutions to mitigate this issue, which can be categorized as active and passive. Filatov et al. [19] introduced a passive approach involving the use of eddy current dampers to provide non-rotating damping to the rotor. Additionally, Tonoli et al. [20] proposed an innovative passive solution, incorporating elastic and dissipative elements between the statoric part of the bearing and the machine's base to address this instability. Moreover, to ensure the stability of EDB across a broad range of speeds, Cui et al. [5] introduced an active solution where EDB was integrated with active magnetic dampers (AMD). A novel homopolar EDB by developed in [21] where axially polarized magnets were utilized. Incontrast in [22] radial magnets were employed there was 450% increase in load bearing capacity. It is necessary to perform sensitivity analysis because there is no proven reference for obtaining initial dimensions of EDB. Determining the important bearing parameters is a time-consuming process, involving a combination of simulations along with experimentation.

Hence, to expedite the development of EDB as well as to save time, investigators are progressively turning to ANN, which has capability to produce superior results without performing experimentation or a large number of simulations. They are capable of handling large numbers of datasets along with they can recognize patterns and trends which helps in predicting the results. ANN is predominantly used in the realm of AMB [23] to enhance control together with increasing operational efficiency.

A novel adaptive control methodology that integrated Backpropagation (BP) neural networks (NN) into proportional-integral-derivative (PID) was developed by Chen et al. [24]. A combination of empirical insights together with the built-in capabilities of BP NN was utilized to determine the ideal number of hidden layers. This approach facilitates real-time modification of PID control variables. Continuous learning from system performance indicators is the foundation of this adaptive approach. This novel approach greatly increases the magnetic bearing system's resistance to outside interference. The working stability of aeromagnetic bearings was improved by applying the radial basis function network by Du and Sun [25]. He et al. [26] aimed to enhance the management of excessively simplified nonlinear components by employing the conventional ''two-step linearization'' technique frequently employed in mathematical models. To address this, they created a nonlinear model based on BP neural networks that aims to provide a more precise illustration of numerous nonlinear attributes and their effects. Tang et al. [27] applied an RBF neural network controller to effectively handle the nonlinear complexities arising from alterations in clearance. These changes give rise to variations in the displacement stiffness of conical rotors, particularly when subjected to significant angular deflections.

While ANN has been widely applied in AMB, the use of ANN in EDB to assess critical bearing characteristics has been notably absent. Insights drawn from an extensive literature review on EDB design yield the following observations.

- EDB has been employed by researchers as a substitute for traditional bearings.
- Thorough sensitivity analysis is necessary to design an EDB. [28]
- The parameters k and c are two fundamental parts of EDB. These variables are essential for performing dynamic and quasi-static simulations. Therefore, it is essential to ascertain these parameters precisely.
- It is not possible to obtain values experimentally during the initial design phase because an EDB prototype is not available. Therefore, using a numerical model is the only practical way to obtain these values..
- With the help of numerical model, crucial variables can be estimated by curve fitting analytical model to numerical results.

As a result, it is difficult for designers to choose the best EDB for each application. These issues could be addressed by creating an ANN model that predicts bearing characteristics of EDB. The research gaps found from a thorough literature review served as the foundation for the work done on this article. To properly fill in these gaps, the research was split into three primary parts. The first part of research focuses on conducting a sensitivity analysis by varying varying diameter of conductor, width of magnet, thickness of magnet, thickness of conductor, airgap and eccentricity. Determining how these variations affected the values of ω, k, and c was the main objective. The creation and training of an ANN model took place in the study's second section. The three different ANN models were trained using the information gathered from the sensitivity analysis carried out in the first phase of the study.

The goal of this training procedure was to find correlations between the input and output variables.

In the third part, Regression model obtained from the ANN was used to optimize EDB. The Bonobo optimizer facilitated the optimization process to attain the best EDB configuration.

The results obtained from optimization was validated with COMSOL Multiphysics and analytical model. After validation, these outcomes were compared with the ANN model's predictions to evaluate the accuracy and dependability of the ANN-based optimization strategy.

II. RADIAL ELECTRODYNAMIC BEARING CONFIGURATION

The rotor receives support radially within the domain of radial EDB. There are two more categories within this one: active and passive configurations. In the case of passive radial EDB, due to the interaction of conductor with a magnetic field originating from a permanent magnet (PM), eddy currents are produced. The stabilizing force for the rotor is provided by this interaction.

Two different types of passive radial EDB can be distinguished by the number of magnetic field reversals that the conductor experiences in a single rotation:

1. Heteropolar Radial EDB (Fig. 1(a)): This type features multiple magnetic field reversals within one rotation.

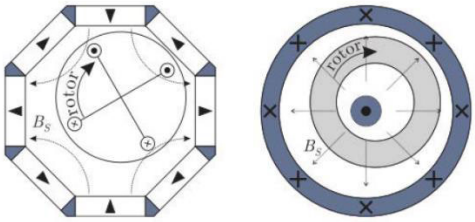

FIGURE 1. Radial EDB configurations: (a) heteropolar and (b) homopolar [29].

2. Homopolar Radial EDB (Fig. 1(b)): In this variant, no magnetic field reversals occur during a rotation.

Usually, solid conducting objects like cylinders or discs make up homopolar rotors. Furthermore, there are two types of homopolar bearings: axial flux and radial flux configurations. The magnetic flux is parallel to the rotating conductor in the axial flux arrangement (Fig. 2(a)). On the other hand, the magnetic flux flows radially through the conductor in the radial flux configuration (shown in Fig. 2(b)).

This paper explores the simulation of the axial flux configuration utilizing COMSOL Multiphysics, with a specific emphasis on the double flux configuration. The attention to the double flux configuration arises from the fact that in axial flux configuration, nearly all magnetic flux is harnessed to generate force.

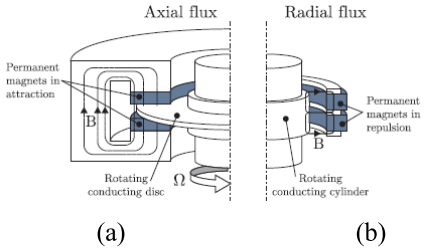

FIGURE 2. Two distinct flux configurations for homopolar EDB (a) axial flux, (b) radial flux [29].

III. MATHEMATICAL MODEL FOR STIFFNESS AND DAMPING COEFFICIENTS

An overview of the mathematical model used to analyze the electromagnetics in EDB is given in this section. Centered on electromechanical dynamics, the EDB model concentrates on a conductor in motion within an unchanging magnetic field. Motional eddy current dampers work similarly to linear voice coils, as shown in Fig. 3, where the coil's electric terminals are bridged by an inductive and resistive load, with R as well as L standing for the coil's resistance and self-inductance. This arrangement is similar to a mechanical system that Amati et al. [11] proposed, in which a viscous damper and a linear spring are connected in a complex series arrangement.

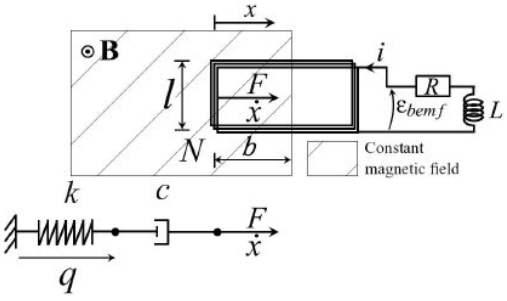

FIGURE 3. Electromechanical model of EDB [28].

When a wire loop moves in the x-direction through a constant magnetic field with flux density B, the electromotive force (emf) can be calculated using Faraday's law. Kirchhoff's voltage law is used to calculate induced eddy currents and the interaction between the generated current and the magnetic field results in the subsequent Lorentz force.

$$F = N \int i\vec{d}l \times \boldsymbol{B} \tag{1}$$

where i is the current flowing through the wire loop, $\boldsymbol{B}$ is the constant magnetic field, N is the number of turns, and F is the Lorentz force.

The forces produced by eddy currents when a conductor rotates radially in an axisymmetric magnetic field are calculated using the Lorentz force equation. The electromagnetic force developed by EDB when the rotor is rotating in a fixed eccentricity i.e. quasi-static is given in equation (2).

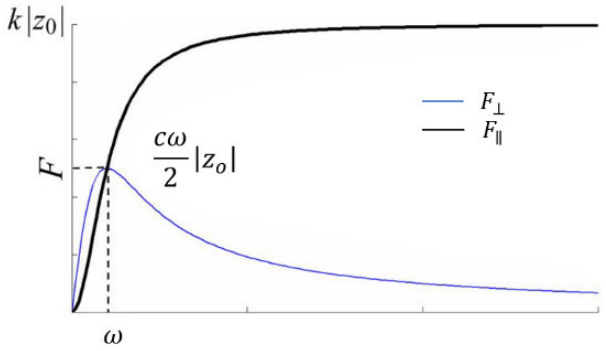

FIGURE 4. Forces generated in EDB, parallel $F_{\|}$, and perpendicular force $F_{\perp}$ [11].

The quasi-static analysis is used to identify the important parameters which have an influence on the stability analysis of EDB.

$$F = \frac{k}{1+\left(\frac{\omega}{\Omega}\right)^2} z_o - j\frac{c\Omega}{1+\left(\frac{\Omega}{\omega}\right)^2} z_o = F_{\|} + jF_{\perp} \tag{2}$$

In equation (2) k is the stiffness, c is damping, ω is electric pole frequency, and Ω is angular speed.

A plot depicting both parallel ($F_{\|}$), perpendicular force $F_{\perp}$ is shown in Fig. 4. It can be observed that, the electric pole of the EDB can be identified as the rotation speed at which $|F_{\perp}|$ is a maximum and damping parameter of the EDB can be identified as $F_{\perp}$ reaches a maximum i.e. $F_{\perp}$max for $\Omega = \omega$:

$$\begin{cases} \Omega_{|F_{\perp}|_{max}} = \omega \\ |F_{\perp}|_{max} = \dfrac{c\omega}{2}|z_o| \end{cases} \tag{3}$$

Magnetic forces produced by EDB are highly dependent on several critical parameters. The exact magnetic arrangement used, the volume where eddy currents interact with the magnetic flux, the magnetic flux density applied to the conductor, and the relative speed between the conductor and the magnetic field all play a major role in determining the characteristics of an EDB. These properties are closely linked to the geometry, bearing configuration, and material properties. FEA has been a widely used method for building EDBs, especially with respect to quasi-static features.

Two critical parameters, denoted as k and c, are crucial to the mechanical equivalent model of the EDB principle within the analytical model. These parameters are critical in both quasi-static and dynamic simulations and must be estimated or determined experimentally. It is not practical to make an experimental determination during the design process if there is no prototype. Consequently, the numerical model presented in Section IV becomes the main method to find these parameters. Hence sensitivity analysis has been performed by utilizing numerical model due to this reason.With the help of this numerical model, a plot can be created, as seen in Fig. 4, which provides the basis for determining the crucial parameters needed for the analytical model. It is possible to calculate the values of k as well as c for the mechanical equivalent of the EDB by examining the identification point where curves intersect.

IV. NUMERICAL MODEL

The characteristics of EDB are primarily determined by numerous factors linked to magnetic force generation. These include the speed at which the conductor traverses in relation to the magnetic field, the strength of the magnetic flux flowing in the direction of the conductor, the location where eddy currents interact with the magnetic flux, and the specific magnetic configuration, whether it be axial or radial. To design an EDB with quasi-static characteristics, FEA has been employed. In this analysis, the parameters k and c have been determined by curve-fitting analytical model to the numerical solutions obtained from the FEA. A sensitivity study was conducted to better understand the impact of various geometric factors on both the electric pole frequency and the bearing's mechanical stiffness. A quasi-static analysis was carried out in order to achieve this goal. The conductor in this test was first rendered immobile before being rotated at a constant angular velocity. The stationary distribution of eddy currents can be determined using a common reference frame for the stator as well as the rotor. This method performs a combined calculation using a single mesh. The validity of this methodology has been confirmed and supported by evidence in Ref [30].

The current distribution (J) in the conductor for EDB and the flux density ($\boldsymbol{B}$) over all domains can be estimated using FEA. The conductor movement is considered by formulation $v \times B$, here, v stands for the conductor's velocity field.

$$v = \begin{Bmatrix} v_x \\ v_y \\ v_z \end{Bmatrix} = \begin{Bmatrix} -y\Omega \\ x\Omega \\ 0 \end{Bmatrix} \tag{4}$$

The Lorentz forces generated can be determined by performing a volume integration of $\boldsymbol{J} \times \boldsymbol{B}$ inside the field of the conductor.

$$F_L = \iiint_{re} J \times \boldsymbol{B} dV \tag{5}$$

During the quasi-static simulation, a minor eccentricity ε was introduced between the EDB magnets' domain as well as the conductor domain, specifically in the x direction, leading to $z = \varepsilon = E$. Here, z is a real number. Through the comparison of Lorentz forces evaluated via the finite analysis method with forces derived from equation (1), direct evaluations can be conducted. The force in the x-direction is denoted by the real part of the Lorentz forces, whereas the force in the y-direction is indicated by the imaginary part.

A. SENSITIVITY ANALYSIS

An established reference for the initial sizing of conductors and magnets in EDB is conspicuously lacking as of this writing. Consequently, there is no easily accessible method to

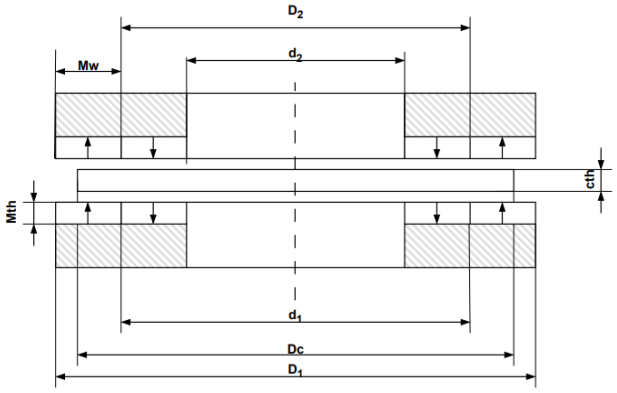

FIGURE 5. Geometrical parameters of EDB used for sensitivity analysis.

TABLE 1. Physical parameters used for numerical analysis.

Parameter	Unit	Value
Electrical conductivity of copper	A/V	5.99×10^7
Magnetic flux density	T	1.2
Permeability of iron	-	4000

calculate the EDB parameters for a given geometry. A thorough sensitivity analysis is required as part of the design process due to this constraint. Through the execution of a thorough sensitivity analysis, a holistic understanding and assessment of the collective impact of various parameters on the system can be attained.

Various analyses are carried out in an effort to determine the optimal geometry of the EDB and determine the most suitable configuration. A reference model was created to offer direction for the analysis, as shown in Fig. 5. The geometrical along with physical properties of the models used in the sensitivity analysis are shown in Tables 1 and 2, respectively.

FE simulations using the AC/DC module in COMSOL Multiphysics were conducted using the data from Table 2. Maintaining the rotor's rotational speed and lining up the conductor's rotational axis with the magnetic field's symmetry axis were necessary to create a quasi-stationary condition. The rotation axis must be deliberately different from the magnetic field's symmetry axis. This arrangement produces a force between the conductor and the magnetic field. The constituent components of the force can be computed using a FE model. The model's parameters can be effectively determined by applying a curve-fitting methodology to eqn. (6) alongside the results of the FE analysis. Special care must be taken while meshing to obtain good approximations. Hexahedral elements have been used to mesh the EDB configuration (Fig. 6).

The EDB simulation employed the design parameters outlined in Table 3. In Fig. 7 to 8, you can see the paths of eddy currents at 5000 RPM and 10000 RPM. They move from the low potential area through the center of the disc and return

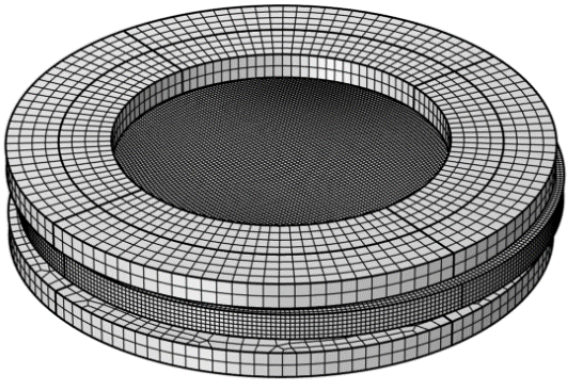

FIGURE 6. FE model of double flux radial EDB configuration.

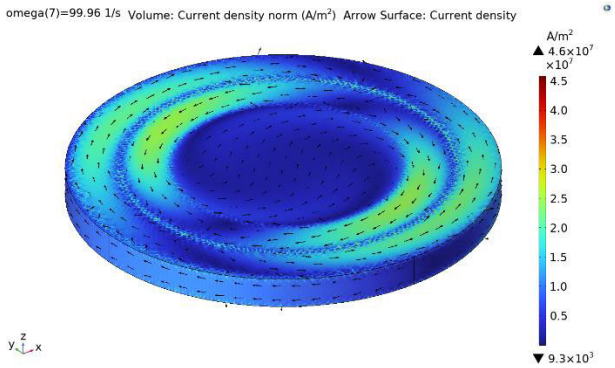

FIGURE 7. Eddy current generated at 5000 rpm.

through the outer part. The way the flux lines behave follows a rule for low-frequency issues (div(J)=0), ensuring that no current leaves the conductor, and there's no external current added. Furthermore, Fig. 9 provides a combined graph displaying the intersection of both forces. Consequently, under quasi-static conditions, the force produced by the double flux EDB can be expressed as:

$$F = \left(\frac{k1}{1 + \left(\frac{\omega_1}{\Omega}\right)^2} + \frac{k2}{1 + \frac{\omega_2}{\Omega}^2} \right) z_{c0} - j \left(\frac{c1 \times \Omega}{1 + \left(\frac{\Omega}{\omega_1}\right)^2} + \frac{c2 \times \Omega}{1 + \left(\frac{\Omega}{\omega_2}\right)^2} \right) z_{c0} \quad (6)$$

B. RESULTS OF SENSITIVITY ANALYSIS

The geometric parameters provided in Table 2 serve as the basis for conducting a sensitivity analysis, and the subsequent section delves into a comprehensive discussion of the results derived from this analysis.

In Figure 10 (a), we can observe the influence of conductor diameter (D) and thickness (cth). An increase in conductor diameter is associated with a decrease in the ω. It is important to highlight that alterations in diameter may jeopardize

TABLE 2. Geometrical variables used for numerical analysis.

Eccentricity (e)	Air gap (g)	Diameter of conductor (Dc)	Thickness of conductor (cth)	Outer diameter of outer magnet (D1)	Inner diameter of outer magnet (d1)	Outer diameter of inner magnet (D2)	Inner diameter of inner magnet (d2)	Thickness of magnet (Mth)	Width of the magnet (Mw)
2.5	2.5	120	10	120	97	97	74	10	23
2	2	115	9	115	91	91	67	9	24
1.5	1.5	110	8	110	85	85	60	8	25
1	1	105	7	105	79	79	53	7	26
0.5	0.5	100	6	100	73	73	46	6	27

TABLE 3. Geometrical parameters used for numerical analysis.

Eccentricity (e)	Air gap (g)	Diameter of conductor (Dc)	Thickness of conductor (cth)	Outer diameter of outer magnet (D1)	Inner diameter of outer magnet (d1)	Outer diameter of inner magnet (D2)	Inner diameter of inner magnet (d2)	Thickness of magnet (Mth)	Width of the magnet (Mw)
1.5	1.5	110	8	110	85	85	60	8	25

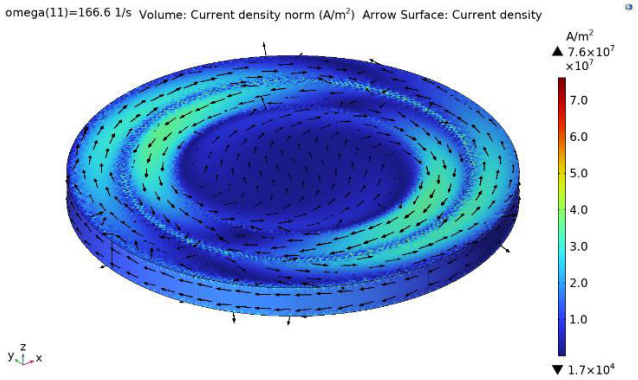

FIGURE 8. Eddy current generated at 10000 rpm.

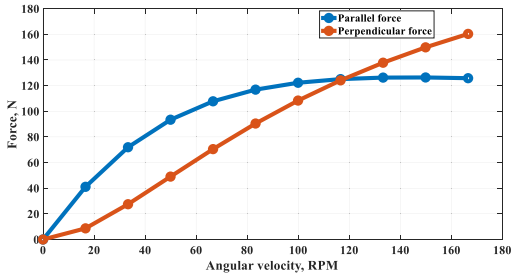

FIGURE 9. Force vs angular velocity.

the stability of the system and have the potential to induce mechanical failures in the conducting disc, attributed to centrifugal forces.

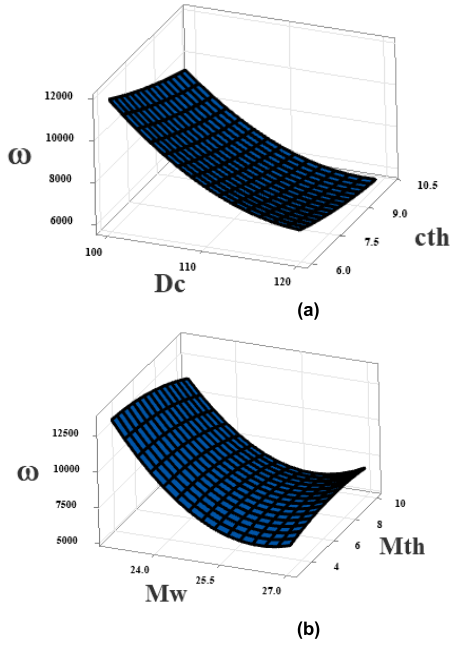

FIGURE 10. Variation of ω, with respect to (a) Dc and cth, (b) Mw and Mth.

On the other hand, when the cth is increased, it leads to a reduction in the ω. This reduction is due to decreased resistance and an increase in reluctance along the magnetic path.

The Fig. 10(b) shows the variation of ω with respect to Mw and Mth. Increasing the width of the magnet reduces

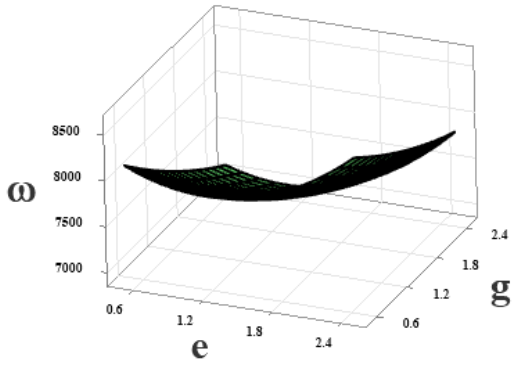

FIGURE 11. Variation of ω with respect to e and g.

the electric pole frequency, because the amount of the eddy current generated in the conductor increases. The variation of electric pole ω with respect to eccentricity and airgap is illustrated in Fig. 11.

The investigation into the effects of various parameters, including conductor diameter, magnet thickness, eccentricity, and airgap, is presented through the graphical representation of stiffness variations ($k1$ and $k2$). These variations are showcased in Figures 12 to 15. The overall stiffness of the EDB can be increased by increasing the conductor diameter, as shown in Fig. 12. However, an increase in conductor diameter will make it more difficult to stabilise the EDB and will also cause the conducting disc to mechanically fail due to centrifugal forces.

The effect of magnet thickness is displayed in Fig. 13. The overall stiffness of the EDB will increase with an increase in magnet thickness. However, since magnets are an integral part of the EDB, adding thickness also causes the EDB's overall weight to increase. which will make it harder for the EDB to stabilize. In Fig. 14, effect of eccentricity on the stiffness is shown. Reduced eccentricity leads to higher stiffness of the EDB. Affect of the airgap on stiffness is shown in Fig. 15. Increase in airgap leads increase in the stiffness, but reduction in the damping coefficient of EDB. Optimal value of airgap is around 1 -1.5mm.

Likewise, the influence of the same set of parameters on damping characteristics ($c1$ and $c2$) is portrayed through Figures 16 to 19. Effect of conductor diameter is shown in Fig. 16. Increase in diameter increases the damping coefficient. The effect of magnet thickness is shown in Fig. 17. Increased thickness of magnet generates stronger eddy currents.

C. OPTIMIZATION USING ARTIFICIAL NEURAL NETWORK

Inspired by the complex networks observed in the human brain, the ANN is a machine-learning method that is incredibly efficient. NN as depicted in Fig. 20, consists of input and output layers in addition to a hidden layer that houses units that transform inputs into a format that can be used by the output layer.

In this research investigation, ANN was harnessed for the purpose of predicting a single output variable predicated on a set of six distinct input variables. Three different ANN models were developed with same input variables.

The ability of ANN to understand non-linear relationships between inputs and outputs led to their selection. Moreover, ANN are capable of learning from data and adapting to new situations through a process called training. ANN models can modify their variables to reduce prediction errors thanks to this training. Their adaptability allows them to perform well in predictive tasks by allowing them to generalise to previously unseen data. Therefore, these factors influence the applicability of ANN. The dataset underwent meticulous importation and integration into the MATLAB platform, where it was thoughtfully randomized to ensure robust data analysis. The input dataset encompassed crucial parameters, comprising the conductor diameter, magnet width, magnet thickness, conductor thickness, eccentricity, and air gap. Correspondingly, the output dataset featured pivotal variables, specifically encompassing electric pole frequency, stiffness coefficients denoted as $k1$ and $k2$, as well as damping coefficients $c1$ and $c2$.To facilitate the analysis, three distinct ANN models were systematically engineered, each expressly tailored to predict one of the three distinctive output variables of interest. The dataset was subjected to meticulous division into distinct training, validation, and testing subsets, aligning with the conventional allocation of 70% for training, 15% for validation, and 15% for testing. Particularly, the ANN model was developed without any data normalization in the initial stages. A feedforward NN was selected, which consisted of a single hidden layer that could hold anywhere between 10 to 15 neurons. The activation function utilized was hyperbolic tangent function.

The organization of these matrices was carefully altered in accordance with the exact number of neurons residing within the hidden layer.

Bayesian Regularization (BR) 'trainbr' was utilized to train NN. The decision was made because of the benefits provided by BR, which include avoiding overfitting of the data and preventing overtraining [31]. The 'trainParam' structure was applied to accurately define the parameters that controlled the training dataset. The results obtained from these evaluations were meticulously scrutinized and the 'plotregression' function presented a graphic representation of the actual and expected outcomes.

To enable understanding and provide a point of reference, table 5 offers a detailed description of input data along with specific functions that are vital in the ANN network's training. In addition, with the help of a series of equations, the research paper provides a succinct picture of the correlation between input and output layers [32].

$$\{J\} = \Phi(\{A\} + [i] \times \{y\}) \tag{7}$$

$$\{X\} = \alpha(\{d\} + [c] \times \{J\}) \tag{8}$$

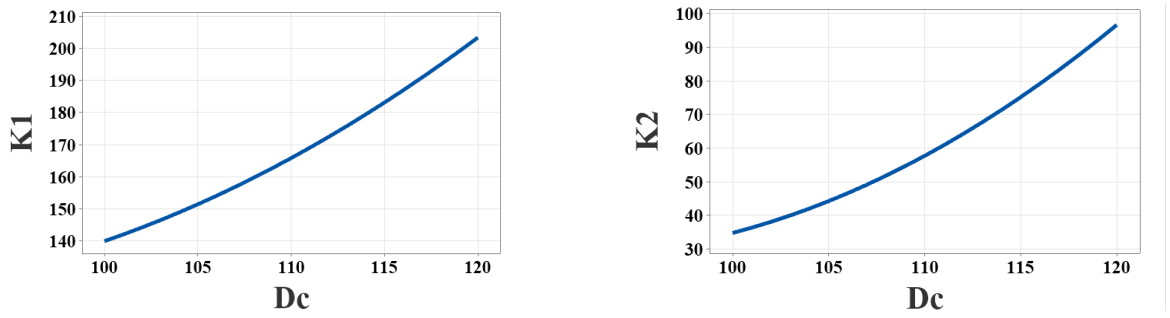

FIGURE 12. Variation of stiffness ($k1$, $k2$) with respect to Dc.

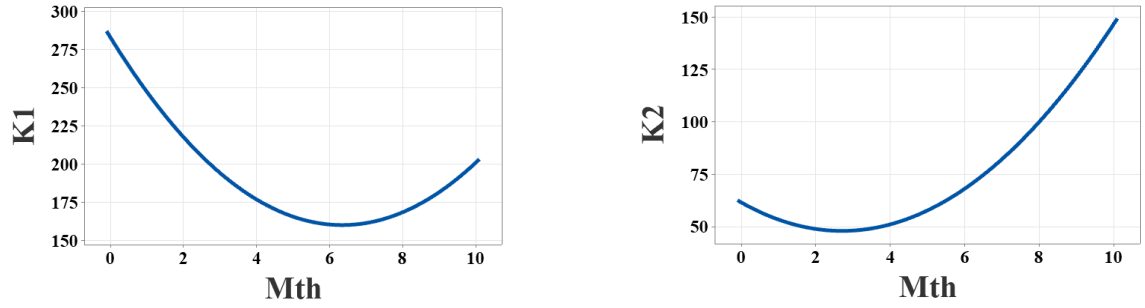

FIGURE 13. Variation of stiffness ($k1$, $k2$) with respect to Mth.

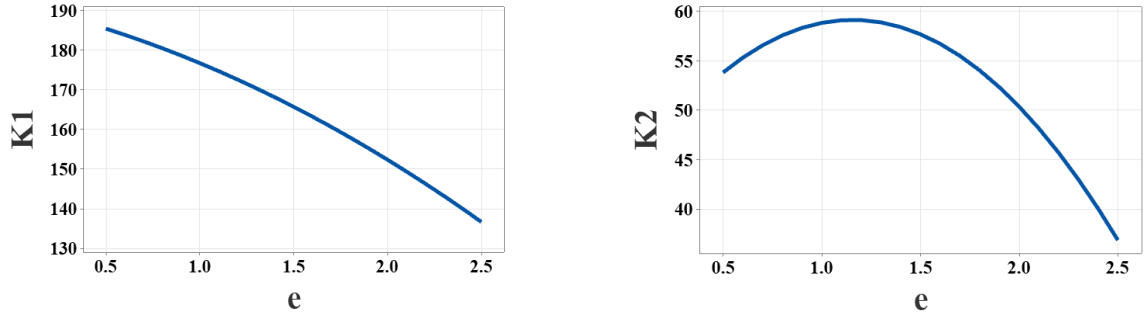

FIGURE 14. Variation of stiffness ($k1$, k 2) with respect to e.

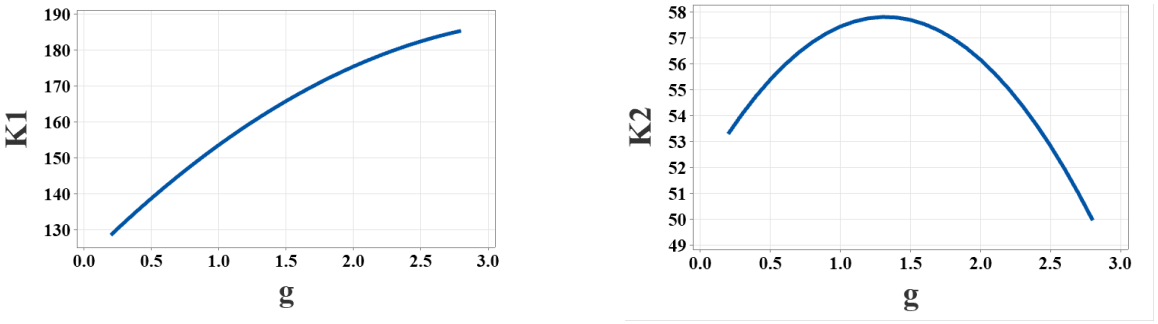

FIGURE 15. Variation of stiffness ($k1$, $k2$) with respect to g.

From this angle, {J} represents the output matrix from the hidden layer, whilst [i] and [c] stand for weight matrices. Meanwhile, {X} indicates the output matrix created by the neural network, with {A} and {d} are bias matrices. The

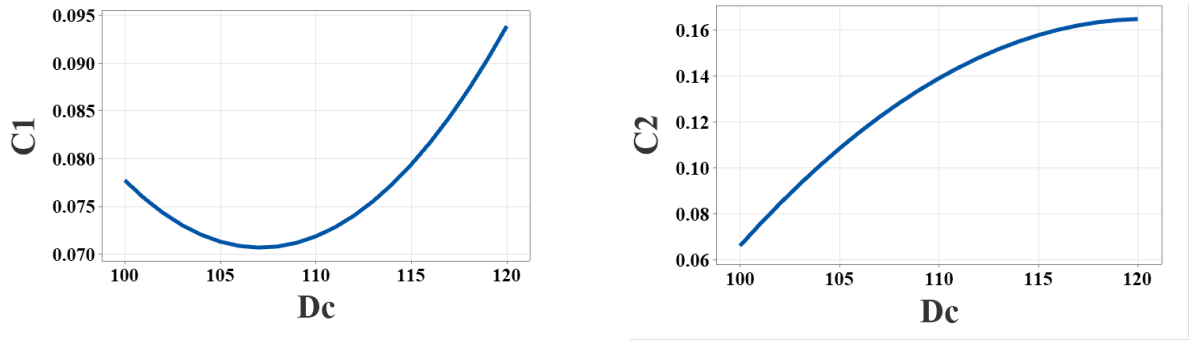

FIGURE 16. Variation of damping ($c1$, $c2$) with respect to Dc.

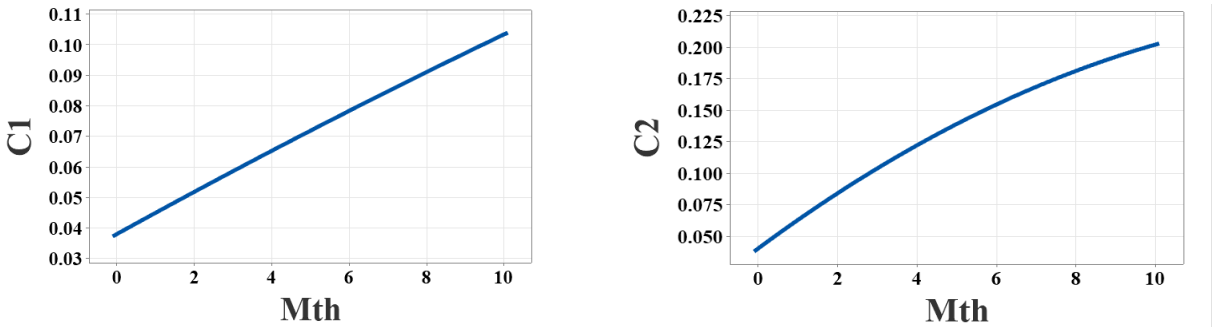

FIGURE 17. Variation of damping ($c1$, $c2$) with respect to Mth.

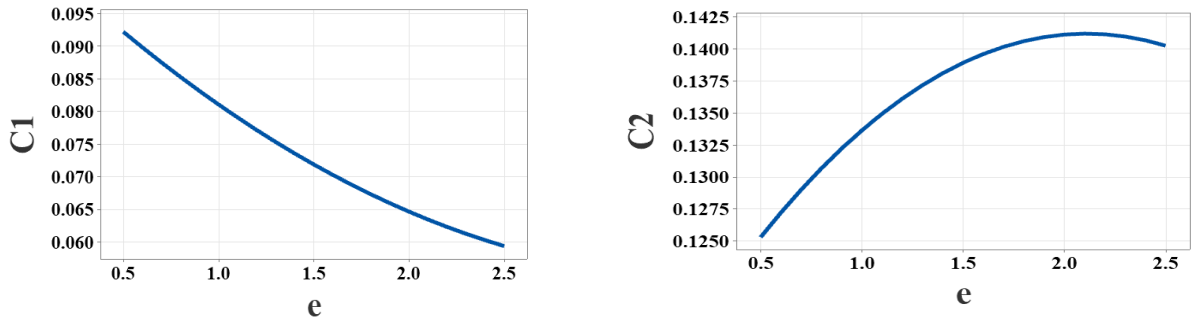

FIGURE 18. Variation of damping ($c1$, $c2$) with respect to e.

activation functions are represented by Φ and α, and {y} contains the input matrix.

The BR algorithm with 10 hidden neurons (HN) achieved the best R-values. A regression plot illustrating the model trained with the BR algorithm and 10 HN is shown in Fig. 24.

Additionally, a high R-value of 0.99465 highlights ANN models' ability to handle unfamiliar data, which is significant in establishing models' applicability throughout different scenarios. The model's outstanding performance is emphasized by its reliable R-value of 0.99465 which makes it suitable for predicting the electric pole frequency of an EDB. Also, with R-values of 0.98 and 0.99, the ANN model emerges as a strong choice predicting both stiffness ($k1$, $k2$) and damping ($c1$, $c2$).

TABLE 4. EDB coefficients obtained from curve fitting.

Mechanical parameters	Value
ω	6997.2 RPM
$k1$	166050.2N/m
$k2$	66348.9N/m
$c1$	64.91 Ns/m
$c2$	153.18 Ns/m

The model's overall excellence is highlighted by its consistent R-value of 0.99465 across all assessments, making it a strong recommendation for predicting the electric pole frequency of an EDB. With R-values of 0.98 and 0.99,

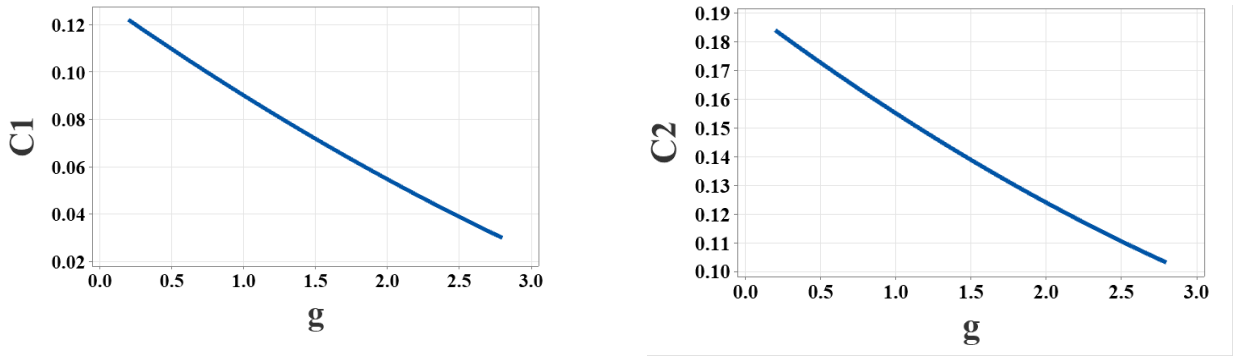

FIGURE 19. Variation of damping (c1, c2) with respect to g.

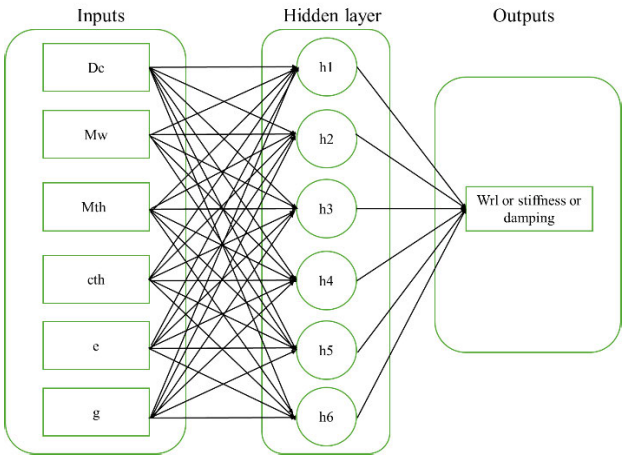

FIGURE 20. Architecture of ANN.

respectively, the model emerges as a robust choice, offering strong recommendations for predicting both stiffness ($k1$, $k2$) and damping ($c1$, $c2$).

The test R-value of 0.9865 highlights the ANN model's ability to handle unknown datasets. This feature is essential to evaluate the model's generalizability. The overall R-value of 0.99465 highlights the quality of the model. Therefore, the developed ANN model can be used to estimate EDB's $\boldsymbol{\omega}$. Comparison between simulated and predicted results is shown in Fig. 21

In Fig. 22, a comparison is presented for predicted and simulated results of stiffness ($k1$, $k2$), while Fig. 23 depicts a similar comparison for damping ($c1$, $c2$).

The regression graphs for the ANN model developed for predicting $\boldsymbol{\omega}$ are shown in Fig. 24. Similarly, the regression graphs for the ANN model developed for predicting the stiffness of electrodynamic bearing are shown in Fig. 25 and for predicting damping are depicted in Fig. 26. The training values in the plot of Fig. 24-26 represent the predictions the ANN model made using the training data. In this process, patterns and relationships that the model learned during training are predicted. Additionally, the prediction made by the ANN model on a separate set of data known as test data is

TABLE 5. Data utilized for ANN network training.

Inputs	Range	Data Employed in MATLAB	Value
Eccentricity	0.5-2.5	Total number of datasets	80
Air gap	0.5-2.5	Number of hidden layers	1
Diameter of the conductor	100-120	Number of hidden neurons used	10
Width of the magnet	23-27	Output	Electric pole frequency, Stiffness($k1$, $k2$), damping($c1$, $c2$)
Thickness of conductor	5-12	Training algorithm used	'trainbr'
Thickness of magnet	3-10		

indicated by test values in the plots. This data, which was not employed in the training phase, helps to understand how the model performed with unknown data. All values in the plot denote results of training and test prediction. This allows to envisage the models overall execution across the whole dataset.

D. OPTIMIZATION OF EDB

In the previous section, the developed ANN model was employed to optimize the EDB. The parameter being optimized was identified as ω. To carry out the optimization process, the Bonobo Optimisation (BO) algorithm was utilized because compared other numerous algorithms BO gave

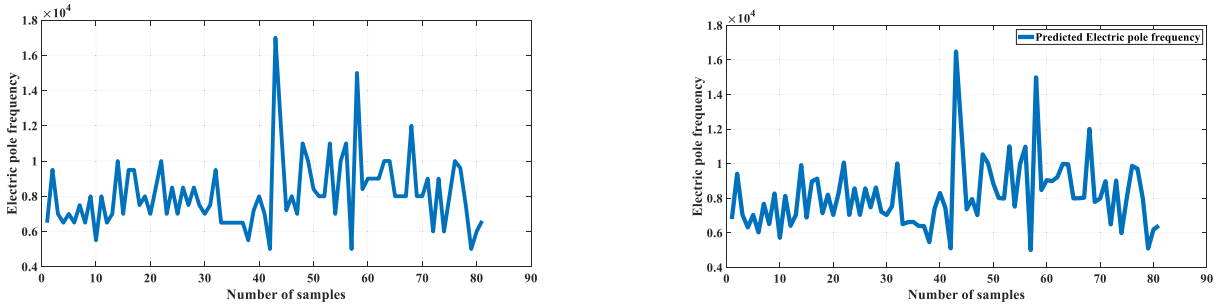

FIGURE 21. Comparison of simulated and predicted outcomes for electric pole frequency.

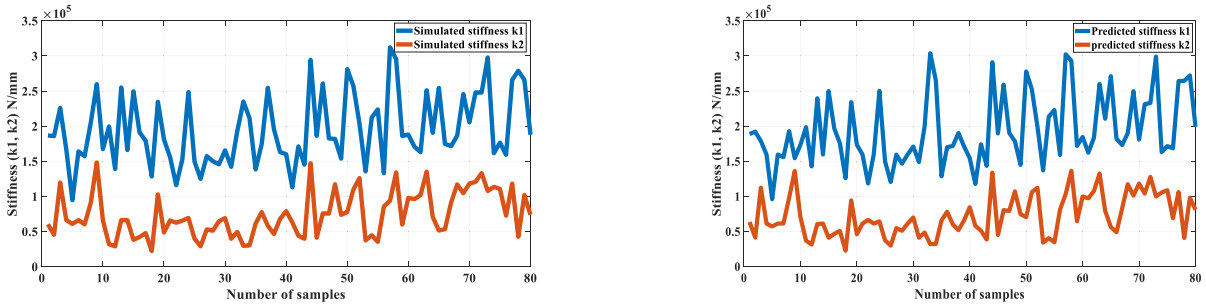

FIGURE 22. Comparison of simulated and predicted outcomes for stiffness ($k1$, $k2$).

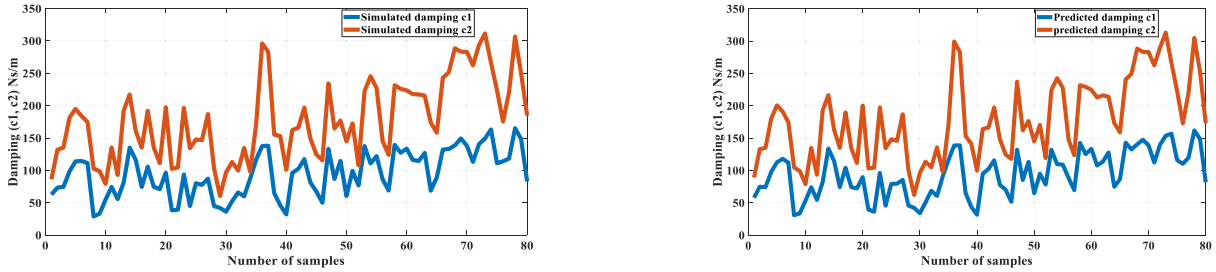

FIGURE 23. Comparison of simulated and predicted outcomes for damping ($c1$, $c2$).

excellent performance [33]. The social behavior and reproductive strategies of bonobos served as the model for this innovative metaheuristic technique. The BO algorithm is based on the fission process, which mirrors the bonobo community's approach of separating into varied subgroups of varying sizes and compositions before reconnecting them with the community.

Furthermore, bonobo ways are divided into four categories: promiscuous, restricted, consortship, along with extra-group mating. The community recognizes each result for all bonobos as the bonobo fitness value, with the alpha bonobo representing the bonobo group's superior alternative.

Initially, the BO algorithm is divided into two phases: positive and negative. The positive phase offers an ideal living scenario, characterized by successful mating, an abundant food supply, and safe living conditions. In contrast, the negative phase shows an unfavorable living environment.

After each iteration of the method, two parameters, positive phase count (P_{pc}) and negative phase count (N_{pc}), are incremented by one. Importantly, when one of these values is adjusted, the other is reset to 0. The selection of bonobos for mating follows a fission–fusion social tactic. The calculation of the greatest size of a temporary sub-group ($Tsgs_{max}$) is determined based on the entire population size (N) employing the equation given by Eq. (8). The selection for $Tsgs_{max}$ is made by considering the maximum value between 2 and the product of $Tsgs_{max}$ and N, where $Tsgs_{max}$ denotes the temporary sub-group size factor.

$$Tsgs_{max} = MAXIMUM(2, Tsgs_{factor} \times N)) \tag{9}$$

The size of the temporary sub-group is randomly defined within the range of 2 and $Tsgs_{max}$. Next, the p^{th} bonobo, recognized as the fittest within the sub-group, is chosen to participate in mating. During the positive phase, there is a higher odds of either restrictive mating or promiscuity,

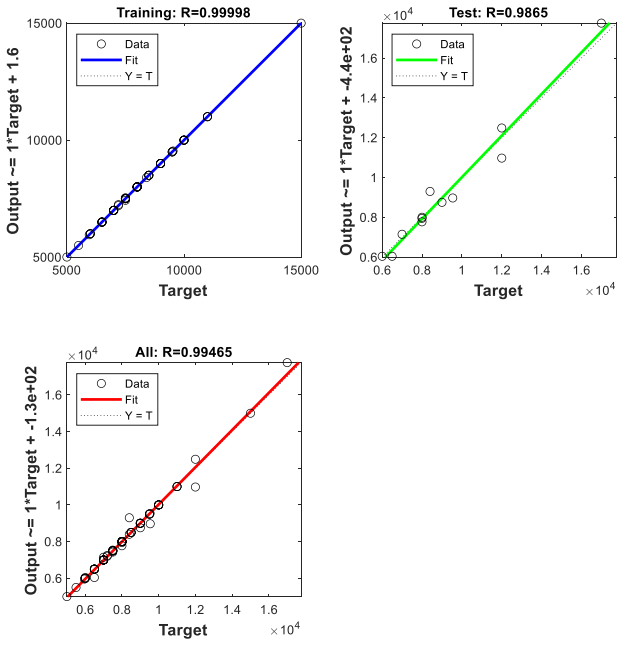

FIGURE 24. Regression plot of ANN model with BR algorithm- 10 HN for electric pole frequency.

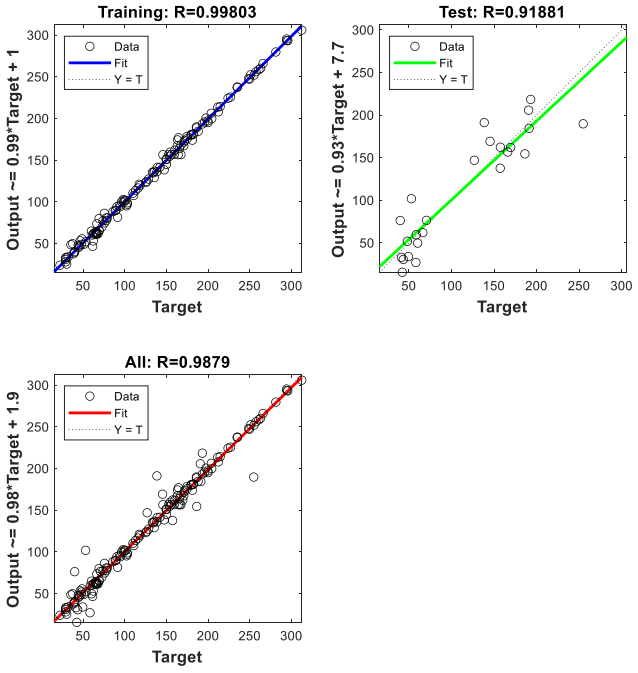

FIGURE 25. Regression plot of ANN model with BR algorithm- 10 HN for stiffness ($k1$, $k2$).

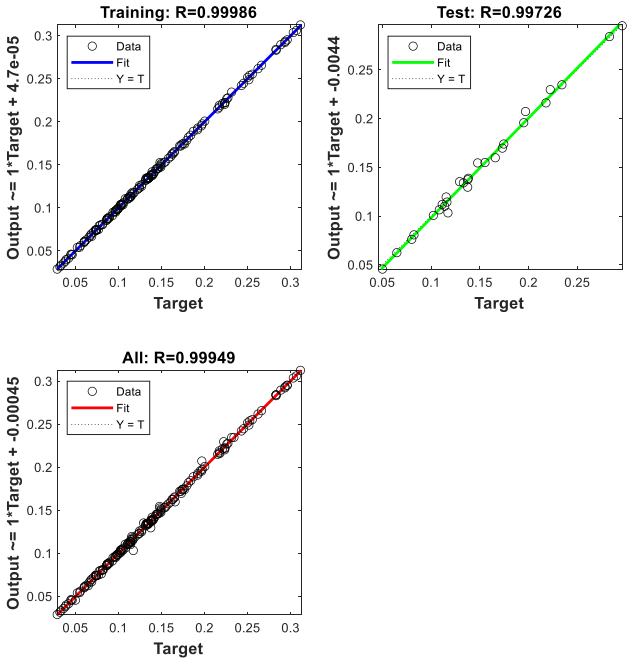

FIGURE 26. Regression plot of ANN model with BR algorithm- 10 HN for damping ($c1$, $c2$).

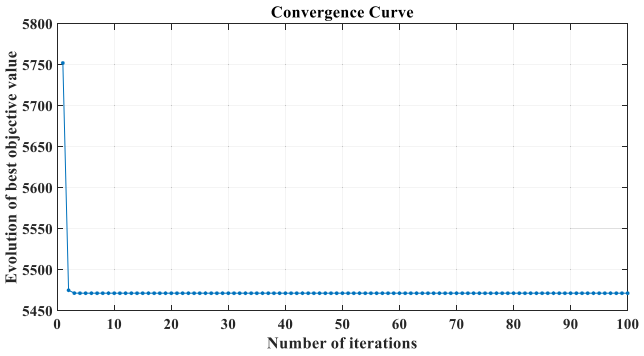

FIGURE 27. The convergence curve of the optimization.

while the negative phase favors a greater likelihood of either extra-group mating or consortship. This probability is denoted as the phase-probability $p_p$in the BO. Initially set to 0.5, p_p is dynamically adjusted after each iteration based on the current phase and phase count number. In a positive phase, p_p ranges from 0.5 to 1.0, whereas during a negative phase, it spans from 0 to 0.5. The fundamental equation governing the positive phase is expressed by Eq. (9).

$$\begin{aligned} New_{bonobo\_J} = {} & Bonobo_J^I + R_1 \times SCAB \\ & \times \left(\alpha_{Bonobo}^J - Bonobo_J^I\right) \\ & + (1 - R_1) \times SCSB \times FLAG \\ & \times (Bonobo_J^I - Bonobo_J^P) \end{aligned} \tag{10}$$

In this context, α_{Bonobo}^J denotes the J^{th} variable of the alpha bonobo, and New_{bonobo_J} represents the J^{th} variable of the offspring. The index J ranges from 1 to d, where d is the amount of parameters in the optimization problem. Furthermore, $SCAB$ and $SCSB$ are parameters associated with sharing. The parameter $FLAG$ is allotted a value of either 1 or -1 depending on a specified condition.

During the negative phase, the generation of the new bonobo takes place through extra-group mating, following the

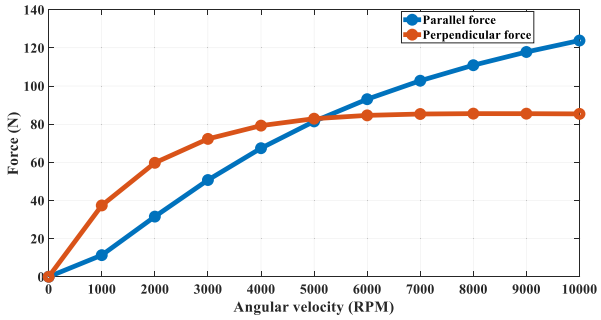

FIGURE 28. Force vs angular velocity.

TABLE 6. Results of the optimization.

Dc	Mw	Mth	cth	e	g	ω
100	27	8	12	1.5	1.5	5445.7

TABLE 7. Comparison of the results obtained from analytical and prediction from ANN.

Bearing characteristics	Analytical with curve fitting	Predicted using ANN	Deviations
Stiffness $k1$	143772.8N/m	148334.9N/m	3.1%
Stiffness $k2$	69768.7N/m	64685.1 N/m	7.2%
Damping $c1$	85.5 Ns/m	90.9 Ns/m	3.8%
Damping $c2$	186.8Ns/m	175.3 Ns/m	6.1%

equations (11) through (16).

$$\beta_1 = e^{\left(r_1^2 + r_1 - \frac{2}{r_1}\right)} \tag{11}$$

$$\beta_2 = e^{\left(-r_1^2 + 2\times r_1 - \frac{2}{r_1}\right)} \tag{12}$$

$$New_{bonobo\_J} = Bonobo_J^I + \beta_1 \times \left(VAR_{MAX\_J} - Bonobo_J^I\right) \tag{13}$$

$$New_{bonobo\_J} = Bonobo_J^I - \beta_2 \times \left(Bonobo_J^I - VAR_{MIN\_J}\right) \tag{14}$$

$$New_{bonobo\_J} = Bonobo_J^I - \beta_1 \times \left(Bonobo_J^I - VAR_{MIN\_J}\right) \tag{15}$$

$$New_{bonobo\_J} = Bonobo_J^I + \beta_2 \times \left(VAR_{MAX\_J} - Bonobo_J^I\right) \tag{16}$$

The convergence curve is shown in Fig. 27. It's evident that fewer iterations were needed to reach the optimal solution. The optimum outcome won't alter if the number of iterations is increased. The optimization results closely align with the outcomes obtained through COMSOL Multiphysics as seen in Fig. 28. The stiffness of the $k1$=143772.8 N/mm and $k1$=69768.7 N/mm and damping is $c1$ =85.5 Ns/m and $c2$ =176.8.8 Ns/m was obtained through curve fitting analytical model. Table 7 presents a comparative analysis of results obtained from the ANN and the analytical model. It is evident that the developed ANN model is versatile, serving both in determining optimal configurations and accurately predicting essential bearing parameters.

V. CONCLUSION

This paper introduces a methodology ANN for the prediction and optimization of EDB. The key conclusions drawn from this study include:

- The application of ANN proves effective in estimating crucial bearing characteristics of EDB.
- Comparative analysis between ANN results and those obtained from an analytical model revealed deviations of 0.44% for electric pole frequency, 3.17 % for stiffness $k1$ and 7.2% for stiffness $k2$ and 3.8% for damping $c1$, 6.1% for damping $c2$.
- To mitigate the need for extensive sensitivity analysis, an ANN regression model was developed. This model streamlines the determination of EDB-bearing features.
- The developed ANN regression model was employed for the optimization of EDB for determining the Dc, Mw, Mth, cth, e, g.
- The validation process for optimization results involved comparison with COMSOL Multiphysics for electric pole frequency. Additionally, the stiffness and damping of the optimized configuration were determined using ANN, and this outcome was further validated using analytical model.

REFERENCES

[1] E. H. Maslen and G. Schweitzer, *Magnetic Bearings*, vol. 53, no. 9. Berlin, Germany: Springer, 2009, doi: 10.1007/978-3-642-00497-1.

[2] S. Earnshaw, "On the nature of the molecular forces which regulate the constitution of the luminiferous ether," *Trans. Cambridge Philos. Soc.*, vol. 7, pp. 97–114, Jan. 1842.

[3] D. K. Supreeth, S. I. Bekinal, S. R. Chandranna, and M. Doddamani, "A review of superconducting magnetic bearings and their application," *IEEE Trans. Appl. Supercond.*, vol. 32, no. 3, pp. 1–15, Apr. 2022, doi: 10.1109/TASC.2022.3156813.

[4] S. I. Bekinal, S. S. Kulkarni, and S. Jana, "A hybrid (permanent magnet and foil) bearing set for complete passive levitation of high-speed rotors," *Proc. Inst. Mech. Eng., C, J. Mech. Eng. Sci.*, vol. 231, no. 20, pp. 3679–3689, Oct. 2017, doi: 10.1177/0954406216652647.

[5] Q. Cui, "Stabilization of electrodynamic bearings with active magnetic-dampers," Ph.D. dissertation, Dept. Robot. Syst. Lab., École Polytechnique Federale de Lausanne, Lausanne, Switzerland, 2016.

[6] S. I. Bekinal, D. Deshwal, and V. G. Srinivas, "Optimized multi-layer radial permanent magnet bearing with an eddy current damping systems," *J. Brazilian Soc. Mech. Sci. Eng.*, vol. 44, no. 11, p. 542, Nov. 2022, doi: 10.1007/s40430-022-03855-7.

[7] D. K. Supreeth, S. I. Bekinal, and S. R. Chandranna, "An overview on electrodynamic bearings," *IEEE Access*, vol. 10, pp. 57437–57451, 2022, doi: 10.1109/ACCESS.2022.3176632.

[8] J. Detoni, "Progress on electrodynamic passive magnetic bearings for rotor levitation," *Proc. Inst. Mech. Eng., C, J. Mech. Eng. Sci.*, vol. 228, no. 10, pp. 1829–1844, Jul. 2014, doi: 10.1177/0954406213511798.

[9] R. F. Post, "Stability issues in ambient-temperature passive magnetic bearing systems," NASA STI/Recon, NASA-Glenn Res. Center, Cleveland, OH, USA, Tech. Rep., 3, 2000.

[10] A. V. Filatov and E. H. Maslen, "Passive magnetic bearing for flywheel energy storage systems," *IEEE Trans. Magn.*, vol. 37, no. 6, pp. 3913–3924, 2001, doi: 10.1109/20.966127.
[11] N. Amati, X. De Lépine, and A. Tonoli, "Modeling of electrodynamic bearings," *J. Vibrat. Acoust.*, vol. 130, no. 6, pp. 1–9, Dec. 2008, doi: 10.1115/1.2981170.
[12] F. Impinna, J. G. Detoni, N. Amati, and A. Tonoli, "Passive magnetic levitation of rotors on axial electrodynamic bearings," *IEEE Trans. Magn.*, vol. 49, no. 1, pp. 599–608, Jan. 2013, doi: 10.1109/TMAG.2012.2209124.
[13] J. Van Verdeghem, C. Dumont, V. Kluyskens, and B. Dehez, "Linear state-space representation of the axial dynamics of electrodynamic thrust bearings," *IEEE Trans. Magn.*, vol. 52, no. 10, pp. 1–12, Oct. 2016, doi: 10.1109/TMAG.2016.2582727.
[14] J. G. Detoni, F. Impinna, A. Tonoli, and N. Amati, "Unified modelling of passive homopolar and heteropolar electrodynamic bearings," *J. Sound Vibrat.*, vol. 331, no. 19, pp. 4219–4232, Sep. 2012, doi: 10.1016/j.jsv.2012.04.036.
[15] C. Dumont, V. Kluyskens, and B. Dehez, "Linear state-space representation of heteropolar electrodynamic bearings with radial magnetic field," *IEEE Trans. Magn.*, vol. 52, no. 1, pp. 1–9, Jan. 2016, doi: 10.1109/TMAG.2015.2475239.
[16] J. Van Verdeghem, V. Kluyskens, and B. Dehez, "Experimental validation and characterisation of a passively levitated electrodynamic thrust self-bearing motor," in *Proc. 21st Int. Conf. Electr. Mach. Syst. (ICEMS)*, Oct. 2018, pp. 1863–1869, doi: 10.23919/ICEMS.2018.8549373.
[17] J. Van Verdeghem, M. Lefebvre, V. Kluyskens, and B. Dehez, "Dynamical modeling of passively levitated electrodynamic thrust self-bearing machines," *IEEE Trans. Ind. Appl.*, vol. 55, no. 2, pp. 1447–1460, Mar. 2019, doi: 10.1109/TIA.2018.2880422.
[18] N. Amati, A. Tonoli, E. Zenerino, J. G. Detoni, and F. Impinna, "Design methodology of electrodynamic bearings," in *Proc. AIAS 38th Nat. Meeting*, 2009, pp. 9–11.
[19] A. Filatov, P. McMullen, K. Davey, and R. Thompson, "Flywheel energy storage system with homopolar electrodynamic magnetic bearing," in *Proc. 10th Int. Symp. Magn. Bearings*, 2006, pp. 21–26.
[20] A. Tonoli, N. Amati, G. Genta, and F. Impinna, "A new stabilization technique for electrodynamic bearings," in *Proc. ISMB*, vol. 12, 2010, pp. 551–560.
[21] A. Alzhrani and K. Atallah, "Novel passive electrodynamic magnetic bearings," in *Proc. IEEE Energy Convers. Congr. Expo. (ECCE)*, Oct. 2022, pp. 1–7, doi: 10.1109/ECCE50734.2022.9947987.
[22] D. Rura, J. Barta, and P. Klima, "Design and analysis of homopolar electrodynamic bearing with radial magnets," in *Proc. Int. Conf. Electr. Mach. (ICEM)*, Sep. 2022, pp. 321–327, doi: 10.1109/ICEM51905.2022.9910773.
[23] F.-J. Lin, S.-Y. Chen, and M.-S. Huang, "Tracking control of thrust active magnetic bearing system via Hermite polynomial-based recurrent neural network," *IET Electric Power Appl.*, vol. 4, no. 9, pp. 701–714, 2010. [Online]. Available: https://digital-library.theiet.org/content/journals/10.1049/iet-epa.2010.0068
[24] S.-Y. Chen and F.-J. Lin, "Decentralized PID neural network control for five degree-of-freedom active magneticbearing," *Eng. Appl. Artif. Intell.*, vol. 26, no. 3, pp. 962–973, Mar. 2013, doi: 10.1016/j.engappai.2012.11.002.
[25] X. Du and Y. Sun, "Control of hybrid electromagnetic bearing and elastic foil gas bearing under deep learning," *PLoS ONE*, vol. 15, no. 12, Dec. 2020, Art. no. e0243107, doi: 10.1371/journal.pone.0243107.
[26] H. He, Y. Liu, and L. Ba, "A nonlinear dynamic model of flywheel energy storage systems based on alternative concept of back propagation neural networks," *J. Comput. Nonlinear Dyn.*, vol. 17, no. 9, p. 91006, Sep. 2022, doi: 10.1115/1.4054681.
[27] J. Tang, X. Zhao, Y. Wang, and X. Cui, "Adaptive neural network control for rotor's stable suspension of Vernier-gimballing magnetically suspended flywheel," *Proc. Inst. Mech. Eng., I, J. Syst. Control Eng.*, vol. 233, no. 8, pp. 1017–1029, Sep. 2019, doi: 10.1177/0959651818813625.
[28] I. Fabrizio, "Electrodynamic bearings," Ph.D. thesis, Dept. Mechtron., Politecnico di Torino, Turin, Italy, 2010.
[29] J. G. Detoni, "Developments on electrodynamic levitation of rotors," Ph.D. dissertation, Dept. Mechtronics Eng., Politecnico di Torino, Turin, Italy, 2012.
[30] J. G. Detoni, Q. Cui, N. Amati, and A. Tonoli, "Modeling and evaluation of damping coefficient of eddy current dampers in rotordynamic applications," *J. Sound Vibrat.*, vol. 373, pp. 52–65, Jul. 2016, doi: 10.1016/j.jsv.2016.03.013.
[31] J. P. S. Rosa, D. J. D. Guerra, N. C. G. Horta, R. M. F. Martins, and N. C. C. Lourenço, *Artificial Neural Networks*, vol. 458. Totowa, NJ, USA: Humana Press, 2009, doi: 10.1007/978-1-60327-101-1.
[32] D. F. Specht, "A general regression neural network," *IEEE Trans. Neural Netw.*, vol. 2, no. 6, pp. 568–576, Nov. 1991, doi: 10.1109/72.97934.
[33] A. K. Das and D. K. Pratihar, "A new bonobo optimizer (BO) for real-parameter optimization," in *Proc. IEEE Region 10 Symp. (TENSYMP)*, Jun. 2019, pp. 108–113, doi: 10.1109/TENSYMP46218.2019.8971108.

D. K. SUPREETH is currently a Research Scholar with the Department of Mechanical and Industrial Engineering, Manipal Institute of Technology, MAHE, Manipal, India. Passive magnetic bearings and optimization are the areas of his expertise.

SIDDAPPA I. BEKINAL is currently a Professor with the Department of Mechanical and Industrial Engineering, Manipal Institute of Technology, MAHE, Manipal, India. Passive magnetic bearings, mechanical vibrations, rotor dynamics, turbomachinery, and mechanical vibrations energy harvesting are the areas of his expertise.

R. C. SHIVAMURTHY is currently an Assistant Professor (Selection Grade) with the Department of Mechanical and Industrial Engineering, Manipal Institute of Technology, MAHE, Manipal, India. Surface engineering, tribology, metal matrix composites, 3D printing, metal processing, materials characterization, and failure analysis are the areas of his expertise.